MOLECULAR AND CELLULAR BIOLOGY, Mar. 2008, p. 1541–1552 Vol. 28, No. 5
0270-7306/08/$08.00+0 doi:10.1128/MCB.01359-07

CARD6 Is Interferon Inducible but Not Involved in Nucleotide-Binding Oligomerization Domain Protein Signaling Leading to NF-κB Activation▽

Almut Dufner,[1]* Gordon S. Duncan,[1] Andrew Wakeham,[1] Alisha R. Elford,[1] Håkan T. Hall,[1] Pamela S. Ohashi,[1,2] and Tak W. Mak[1,2]

Campbell Family Institute for Breast Cancer Research and Ontario Cancer Institute, Toronto, Ontario, Canada M5G 2C1,[1] *and Departments of Medical Biophysics and Immunology, University of Toronto, Toronto, Ontario, Canada M5S 1A8*[2]

Received 28 July 2007/Returned for modification 31 August 2007/Accepted 17 December 2007

We have previously reported the cloning and characterization of CARD6, a caspase recruitment domain (CARD)-containing protein that is structurally related to the interferon (IFN)-inducible GTPases. CARD6 associates with microtubules and with receptor-interacting protein 2 (RIP2). RIP2 mediates NF-κB activation induced by the intracellular nucleotide-binding oligomerization domain (NOD) receptors that sense bacterial peptidoglycan. Here we report that the expression of CARD6 and RIP2 in bone marrow-derived macrophages is rapidly induced by beta IFN and gamma IFN. This IFN-induced upregulation of CARD6 is suppressed by lipopolysaccharide (LPS), in contrast to LPS's enhancement of IFN-induced RIP2 upregulation. We generated CARD6-deficient (CARD6$^{-/-}$) mice and carried out extensive analyses of signaling pathways mediating innate and adaptive immune responses, including the NOD pathways, but did not detect any abnormalities. Moreover, CARD6$^{-/-}$ mice were just as susceptible as wild-type mice to infection by *Salmonella enterica* serovar Typhimurium, *Listeria monocytogenes*, *Candida albicans*, lymphocytic choriomeningitis virus, or mouse adenovirus type 1. Thus, although structural and in vitro analyses strongly suggest an important role for CARD6 in immune defense, the physiological function of CARD6 remains obscure.

The caspase recruitment domain (CARD) is a homotypic protein-protein interaction module that links components of signal transduction pathways implicated in the regulation of apoptosis or adaptive or innate immunity (2, 37). Although much progress has been made in assigning precise roles to most CARD-containing proteins, the functions of the 1,037-amino-acid (aa) human and 1,175-aa mouse CARD6 proteins are still unknown. CARD6 has a unique structure in that it contains the CARD at the N terminus, a glutamic acid-rich region following the CARD, and a proline-rich region at the C terminus (7). CARD6 also harbors a ~350-aa region with similarity to upregulated gene 4 (URG4), a protein that is induced in response to hepatitis Bx antigen overexpression and exerts a positive effect on proliferation (36). Both CARD6 and URG4 share structural features with members of the multifaceted, interferon (IFN)-inducible GTPase (IFNiGTPase) superfamily, which contains some of the proteins most abundantly induced during cell-autonomous immune responses (6).

We are only now beginning to understand the functions of the IFNiGTPases (reviewed in reference 24). The Mx proteins were among the first IFNiGTPases identified and were shown to comprise cell-autonomous factors conferring resistance to viral infection (13). Three other groups of IFNiGTPases are the p47 GTPases, the guanylate-binding-protein GTPases, and the very large inducible GTPases (VLIGs). Members of the p47 GTPase family interact with phagocytic and secretory pathways to oppose infection by enforcing disposal and presentation of bacterial and protozoan antigens (22). The functions of the guanylate-binding proteins and the VLIGs are still not clear. The prototypical VLIG is VLIG-1, a 280-kDa cytosolic and nuclear protein that is strongly induced by IFNs (16). Several factors suggest that VLIG-1, URG4, and CARD6 belong to the same novel subfamily related to the IFNiGTPases (6): (i) all three proteins share regions of significant homology; (ii) all three proteins possess an inosine-5′-monophosphate dehydrogenase domain; and (iii) VLIG-1 and the structurally similar C-terminal regions of CARD6 and URG4 are each encoded by one large exon.

Our initial characterization of human CARD6 showed that this protein associates with microtubules in a CARD- and proline-rich region-dependent manner (7). CARD6 also interacts with RIP2 (also known as RICK or CARDIAK), a CARD-containing member of the RIP family of protein kinases (25). RIP2 mediates NF-κB activation induced by the engagement of the intracellular peptidoglycan receptors nucleotide-binding oligomerization domain containing 1 (NOD1) and NOD2 (3, 14, 17).

Interestingly, the CARD of CARD6 negatively controls both the coimmunoprecipitation of CARD6 and RIP2 and a covalent modification of RIP2. Conversely, the CARD of RIP2 mediates the translocation of CARD6 to aggresomes (7). Moreover, human CARD6 enhances NK-κB activation mediated by several independent pathways. These findings suggest that CARD6 and RIP2 interact at microtubules to modify each other's localization and perhaps enzymatic properties, which ultimately affects the coimmuniprecipitation of both molecules (7). CARD6's structural similarity to the IFNiGTPases supports the hypothesis that CARD6 and RIP2 are likely involved in microtubular transport or sequestration mechanisms during cell-autonomous immune responses. Others have described a

* Corresponding author. Mailing address: Campbell Family Institute for Breast Cancer Research and Ontario Cancer Institute, Toronto, Ontario M5G 2C1, Canada. Phone: (416) 946 2234. Fax: (416) 204 5300. E-mail: a_dufner@yahoo.com.

▽ Published ahead of print on 26 December 2007.

truncated form of human CARD6 that has been named CINCIN1 after its proposed function: CARD-containing inhibitor of NOD1 and CARDIAK-induced NF-κB activation (35). CINCIN1 contains 280 aa of the CARD6 N terminus fused to 30 aa homologous to an Alu element (35).

Here we report that both CARD6 and RIP2 expression are induced in bone marrow-derived macrophages (BMDMs) by IFNs. To determine the physiological function of CARD6, we generated CARD6-deficient mice and performed extensive analyses of the immune system of these mutants. Our results do not support a role for CARD6 in signaling pathways that have been suggested previously to involve RIP2 or CINCIN1. Moreover, CARD6-deficient mice were normally resistant to infection by a broad range of pathogens. This finding argues against a unique role for CARD6 in cell-autonomous immune responses, despite CARD6's structural similarity to the IFNiGTPases. The physiological function of CARD6 thus remains to be determined.

MATERIALS AND METHODS

Generation of CARD6-deficient mice. A genomic CARD6 clone was isolated by screening the RPCI-21 129 mouse P1-derived artificial chromosome library (27) and used to construct a targeting vector that was electroporated into E14K embryonic stem (ES) cells. Clones resistant to G418 were selected, and recombinants were identified by PCR and Southern blotting. Three independent ES clones carrying the floxed CARD6 allele (see Fig. 1) were obtained and microinjected into C57BL/6 blastocysts to generate chimeric mice. These mice were then crossed to Cre-transgenic mice to achieve ubiquitous deletion of the loxP-flanked gene segment (32) and to C57BL/6 mice to generate CARD6$^{+/-}$ mice. These animals were backcrossed six to eight times into the C57BL/6 background to produce the mice used in most experiments. The experiments shown in Fig. 2, 4, and 5A to C were performed with mice of a mixed background. Sex-matched littermates were used in all experiments except for the survival studies, which were performed with age- and sex-matched mice. All animals were housed and maintained in accordance with the protocols of the Ontario Cancer Institute Animal Care Committee.

Southern blotting, Northern blotting, and real-time PCR. A ^{32}P-labeled exon 3-specific probe for Southern blotting was generated using the following primers: 5′-CTAGATCTGAGAGCTTTGAAGTTCTTCACC-3′ (sense) and 5′-GGAG GTTACTCTTTAACTAGAGACTTGTCG-3′ (antisense). The exon 4-specific probe for Northern blotting was generated using the following primers: 5′-CC ACACGTTTTCCAGAAACC-3′ (sense) and 5′-TGGAGGGCAGCTTGAAG GGC-3′ (antisense). For reverse transcription (RT)-PCR, 0.3 to 0.4 μg RNA was incubated with Reverse Transcriptase Superscript 3 (Invitrogen) and oligo(dT) according to the manufacturer's protocol. PCR to confirm successful gene targeting (40 cycles, 58°C annealing temperature) was performed with HotStarTaq polymerase (Qiagen) and the following CARD6 primers: 5′-TCCATTCCCCC ATCAGAATA-3′ (sense) and 5′-GCCTTCCCTGTGTTGTTTGT-3′ (antisense).

Real-time PCR was performed using the SYBR green PCR master mix (Applied Biosystems) according to the manufacturer's protocol and using the following primers: for CARD6, 5′-AATGCCTTTCCAGAGTCAGC-3′ (sense) and 5′-TTCACCCCCACAGTCTCTTC-3′ (antisense); for RIP2, 5′-CCCTCTG CTTCATCATGACC-3′ (sense) and 5′-ATGCGCCATTTTGATAAACC-3′ (antisense); for double-stranded-RNA-activated protein kinase (PKR), 5′-TGG CAGAACTCAATCACGTC-3′ (sense) and 5′-AATAAAGAGGCACCGGGT TT-3′ (antisense); for TATA-binding protein (TBP), 5′-GCACAGGAGCCAA GAGTGAA-3′ (sense) and 5′-TCACAGCTCCCCACCATGTT-3′ (antisense).

The real-time analysis was carried out with an ABI Prism 7900HT apparatus (Applied Biosystems) and consisted of 10 min of initial denaturation at 95°C, followed by 40 thermal cycles of 15 s at 95°C and 60 s at 60°C. The TBP gene was used as a reference gene for the normalization of expression data. The PCR products were confirmed by sequencing. A dissociation profile was obtained at the end of each analysis to confirm the specificity of the PCR amplification.

Cell culture. Primary CARD6$^{-/-}$ mouse embryonic fibroblasts (MEFs) were cultured in Dulbecco's modified Eagle's medium containing 10% fetal calf serum (FCS), 100 μg ml^{-1} penicillin-streptomycin, and 0.1% β-mercaptoethanol. T and B cells were maintained in RPMI 1640 medium containing 10% FCS, 100 μg ml^{-1} penicillin-streptomycin, and 0.1% β-mercaptoethanol.

Generation and stimulation of BMDMs and BMDCs. For the generation of both BMDMs and bone marrow-derived dendritic cells (BMDCs), bone marrow from tibias and femurs was obtained by flushing with phosphate-buffered saline (PBS) containing 1% FCS and depleted of red blood cells using RBC lysis buffer (Sigma Aldrich). For BMDMs, bone marrow was seeded into standard tissue culture plates containing RPMI supplemented with 10% FCS and 50 ng ml^{-1} macrophage-stimulating factor (R&D Systems). At 12 h postseeding, unattached bone marrow cells were recovered and transferred to ultra-low-attachment tissue culture plates (Corning) and cultured for 6 days in the above medium. At day 6, BMDMs were recovered and seeded into flat-bottom 96-well plates at a density of 0.5×10^6 cells ml^{-1}. The cells were then stimulated for 24 h with 100 ng ml^{-1} ultra-pure *E. coli* lipopolysaccharide (LPS) (LPSp; ligand for Toll-like receptor 4 [TLR4]; InvivoGen), 1 μg ml^{-1} Pam_3CSK4 (synthetic ligand for TLR2; InvivoGen), 100 μg ml^{-1} poly(IC) (ligand for TLR3; Amersham), 2.5 μM CpG oligonucleotide ODN 1826 (ligand for TLR9; InvivoGen), 10 μg ml^{-1} muramyldipeptide (MurNAc-L-Ala-D-isoGln; ligand for NOD2; InvivoGen) (MDP), 10 μg ml^{-1} MDP D-D-isomer control (InvivoGen), or 1 μg ml^{-1} γ-D-glutamyl-*meso*-diaminopimelic acid (ligand for NOD1; a kind gift of R. J. Ulevitch, The Scripps Research Institute, La Jolla, CA) (iE-DAP) in the absence or presence of 1 ng ml^{-1} LPS or 50 ng ml^{-1} recombinant mouse gamma IFN (IFN-γ) (Invitrogen). Culture supernatants were collected, and levels of tumor necrosis factor alpha (TNF-α), interleukin 6 (IL-6), and IL-1β were measured by enzyme-linked immunosorbent assay (ELISA) (R&D Systems). Stimulation of BMDMs for quantification of CARD6 RNA and protein levels or the evaluation of signaling pathways by Western blotting was performed using six-well culture dishes. If not indicated as "LPSp", the LPS used in the stimulation experiments was from Sigma (L3012), as were alpha IFN (IFN-α) (100 U ml^{-1}; Sigma) and beta IFN (IFN-β) (100 U ml^{-1}; Sigma).

For BMDCs, bone marrow cells were cultured in RPMI-1640 containing 10% FCS (low-endotoxin, filtered; Gibco), 2 mM L-glutamine, 100 μg ml^{-1} penicillin-streptomycin, and 0.1% β-mercaptoethanol in the presence of 20 ng ml^{-1} granulocyte-macrophage colony-stimulating factor (Peprotech). Immature BMDCs were cultured for 6 days in the above medium. At day 6, the cultures received the same stimuli at the same concentrations as described for the stimulation of BMDMs.

Flow cytometric analyses. Expression of surface markers on thymocytes, splenocytes, BMDCs, and lymph node and bone marrow cells was analyzed using antibodies from BD Pharmingen, a flow cytometer (FACScalibur; Becton Dickinson, San Jose, CA), and CellQuest software according to standard protocols.

T- and B-cell purification and stimulation. For the proliferation experiments, CD4$^+$ T cells and B cells were purified using magnetic beads (Dynabeads; Dynal). For T-cell proliferation assays, round-bottomed 96-well plates were precoated overnight at 4°C with 10 μg ml^{-1} anti-hamster immunoglobulin G (IgG) (307-005-003; Jackson ImmunoResearch Laboratories) and incubated the next day with 100 ng ml^{-1} anti-CD3 (145-2C11; BD Pharmingen). Purified T cells (5×10^4 to 10^5) were added to each well and activated by the plate-bound anti-CD3 alone or by plate-bound anti-CD3 plus anti-CD28 (100 ng ml^{-1}; 553294; BD Pharmingen). Alternatively, T cells were plated in round-bottomed 96-well plates and stimulated with 10 ng ml^{-1} 12-*O*-tetradecanoyl-phorbol 13-acetate (TPA) (Sigma) plus 50 ng ml^{-1} Ca^{2+} ionophore A23187 (Sigma). Purified B cells (5×10^4 to 10^5) were stimulated by incubation with 5 μg ml^{-1} anti-IgM (115-006-020; Jackson ImmunoResearch Laboratories) with or without 5 μg ml^{-1} anti-CD40 (553787; BD Pharmingen), 20 μg ml^{-1} LPS (L3012; Sigma), or 100 nM phosphorothioate-stabilized CpG oligonucleotide ODN 1668 (34). Both T and B cells were harvested at the times indicated in Fig. 4A after an 8-h pulse with [^{3}H]thymidine (1 μCi per well; Amersham). [^{3}H]thymidine incorporation was measured using a Matrix 96 direct β counter system (Canberra Packard). If splenocytes were fractionated for the preparation of protein lysates, T and B cells were isolated with BD IMag Streptavidin Particles Plus-DM after exposure to anti-mouse CD16/CD32 monoclonal antibody (BD Pharmingen) and subsequent incubation with biotinylated anti-T-cell receptor beta (anti-TCR-β) or anti-CD19 antibody (BD Pharmingen), respectively. Purified T cells were activated by preincubation with anti-CD3 plus anti-CD28 (10 μg ml^{-1} each) for 30 min on ice and stimulated for the times indicated in Fig. 4B at 37°C with prewarmed goat anti-Syrian hamster IgG (20 μg ml^{-1}; Jackson ImmunoResearch Laboratories).

T_H1/T_H2 differentiation. For in vitro T_H differentiation assays, single-cell suspensions prepared from spleens were depleted of red blood cells using RBC lysis buffer (Sigma-Aldrich). Splenocytes were plated at 10^6 cells ml^{-1} and stimulated with plate-bound anti-CD3 antibody (200 ng ml^{-1}) as described above. The differentiation of T_H1 or T_H2 cells was initiated by the addition of 5 μg ml^{-1}

anti-IL-4 (554432; BD Pharmingen) or 5 μg ml^{-1} anti-IFN-γ (554408; BD Pharmingen), respectively. After 18 h, IL-2 (50 U ml^{-1}; eBioscience) was added to T_H1 cultures, while both IL-2 (50 U ml^{-1}) and IL-4 (500 U ml^{-1}; Biosource International) were added to T_H2 cultures. Cells were then cultured for 7 days before being harvested, washed, and restimulated for 24 h with plate-bound anti-CD3 (200 ng ml^{-1}), IL-12 (10 ng ml^{-1}; BioSource International), or IL-18 (10 ng ml^{-1}; BioSource International) or a combination of IL-12 plus IL-18. Culture supernatants were collected, and levels of IFN-γ and IL-4 were measured by ELISA (R&D Systems).

Thymocyte apoptosis. Freshly isolated thymocytes were plated at 1×10^6 cells ml^{-1} in 24-well plates and stimulated for 24 h with FasL plus enhancer (54A-001-KI01; Apotech), anti-CD3 (145-2C11; BD Pharmingen), staurosporine (Sigma), λ-irradiation, or UV irradiation at the concentrations and intensities indicated in Fig. 2. Viability was determined by 7-aminoactinomycin D staining and flow cytometry.

LCMV infection and CTL activity. Wild-type (WT) and CARD6$^{-/-}$ mice were injected intravenously with 2,000 PFU lymphocytic choriomeningitis virus (LCMV) (Armstrong strain). At day 3 postinfection, spleens were homogenized and viral titers were determined by plaque assay as described previously (1). At day 8 postinfection, splenocytes were prepared and ex vivo cytotoxic T-lymphocyte (CTL) activity was measured by a standard ^{51}Cr release assay using ^{51}Cr-labeled mouse lymphoma EL4 cells pulsed with the LCMV glycoprotein peptide GP33 or control peptide AV. The number of LCMV-specific CTLs was determined by flow cytometry using labeled anti-CD8 antibody and the GP-33 tetramer.

Pathogen susceptibility. Age- and sex- matched groups of WT and CARD6$^{-/-}$ mice were infected intraperitoneally with *Salmonella enterica* serovar Typhimurium strain SL1344 (kindly provided by J. H. Brumell, Hospital for Sick Children, Toronto, Canada) or intravenously with *Listeria monocytogenes* strain 10403S (kind gift of T. H. Watts, University of Toronto) or with *Candida albicans* strain T117 (kindly provided by J. B. Anderson, University of Toronto). The injected concentrations (CFU) of each pathogen are indicated in Fig. 6A, B, and D. Mice were assessed daily for 2 to 3 weeks to determine their survival and general health. For quantification of *Listeria* organ loads, mice were injected intravenously with 108,000 CFU bacteria and spleens and livers were homogenized at day 3 postinfection in PBS containing 0.2% NP-40. Serial dilutions were plated on brain heart infusion agar, and bacterial colonies were counted the next day. Blood was also collected from infected mice and analyzed for levels of IL-6, IL-12p70, and IFN-γ using the Pierce Biotechnology Searchlight sample testing service. To determine *Candida albicans* titers, mice were injected intravenously with 79,000 CFU and organs were homogenized at day 3 postinfection in PBS. Serial dilutions were plated on BBL CHROMagar Candida plates (BD Diagnostic Systems), and colonies were counted after 2 days. For systemic mouse adenovirus type 1 (MAV-1) infection, mice were injected intraperitoneally with 1,000 PFU MAV-1 virus (kindly provided by K. R. Spindler, University of Michigan, Ann Arbor). On day 3 postinfection, DNA from spleens and brains was extracted using the High Pure PCR template preparation kit (Roche) according to the manufacturer's instructions. To assess the relative MAV-1 DNA content in the infected organs, real-time PCR was performed using 50 ng DNA and the primers described in reference 19.

Western blot analysis. Cells were lysed in 1% Nonidet P-40 lysis buffer (50 mM Tris-HCl, pH 7.5, 120 mM NaCl, 25 mM NaF, 40 mM β-glycerophosphate, 1 mM sodium vanadate, 1 mM benzamidine, 1 μg ml^{-1} aprotinin, 1 μg ml^{-1} leupeptin, 0.2 mM phenylmethylsulfonyl fluoride, 1% Nonidet P-40). Western blot analysis was performed using antibodies recognizing phospho-mitogen-activated protein kinase (MAPK) family members (no. 9910; Cell Signaling), IκBα (no. 9242; Cell Signaling), or phospho-IκBα (Ser32) (no. 9241; Cell Signaling). Proteins were visualized using secondary horseradish peroxidase-coupled anti-rabbit antibody (Amersham) followed by ECL (Amersham). The polyclonal antibody raised against endogenous mouse CARD6 has been described previously (7). Endogenous RIP2 was detected with polyclonal anti-RIP2 antibody (no. 160785-1EA; Cayman) and actin with rabbit antiactin antibody (A-2066; Sigma). Hemagglutinin (HA)-tagged proteins were detected with rat anti-HA 3F10 (Roche Applied Science) antibody.

Assessment of phagolysosomal fusion and pathogen uptake. BMDMs (0.5×10^6 cells/well) were plated on coverslips in six-well standard tissue culture plates. After 18 h, the cells were stimulated with IFN-γ (50 ng ml^{-1}) for 3 h and labeled with 100 nM LysoTracker Red DND-99 (Molecular Probes) for 30 min. Labeled cells were washed three times in PBS and cultured in serum-free RPMI containing 100 nM LysoTracker Red and 50 ng ml^{-1} IFN-γ. *Escherichia coli* (K-12 strain; 6×10^7), *Staphylococcus aureus* (6×10^7), or zymosan A (2×10^7) BioParticles conjugated to Alexa Fluor 488 were added to the plates, followed by centrifugation at 2,000 rpm for 1 min. After 1 h of incubation at 37°C, the cells were washed in cold PBS and fixed in 3% paraformaldehyde in PBS for 10 min. Coverslips were then washed with PBS, DNA was counterstained with 1 μg ml^{-1} 4′,6′-diamidino-2-phenylindole (Sigma), and the coverslips were mounted in Vectashield H-1000 medium (Vector Laboratories). Images were obtained with a Zeiss LSM510 confocal laser scanning microscope. For BMDM pathogen uptake experiments, BMDMs were incubated at 37°C for 1 h with the BioParticles, which were either left untreated or opsonized with opsonizing reagents according to the manufacturer's instructions. The CD11c-positive population of BMDMs was isolated by fluorescence-activated cell sorting and examined for incorporated particles. Extracellular BioParticles were quenched with 1 mg ml^{-1} trypan blue.

Constructs, transfections, and luciferase assay. The moCARD6(D550A)-FLAG and moCARD6(D379A)-FLAG expression constructs were generated from mouse WT-CARD6 in pFLAG-CMV5α (7) by site-directed mutagenesis using the QuickChange mutagenesis system (Stratagene). C-terminally HA-tagged expression constructs for RIP2 and caspase-1 in pcDNA3.1/zeo(−) were generated as described previously (7). Transfections were performed with the FUGENE 6 transfection reagent (Roche). For assessment of NF-κB activation with a luciferase reporter construct, cells were plated in standard six-well culture dishes at subconfluent density and transfected with a total of 2 μg of either empty vector or the pcDNA3-NOD1-HA expression construct in the presence of 200 ng pBVIx-Luc plus 200 ng pRL-TK (Promega). NF-κB activation was assessed at 24 h posttransfection using a dual-luciferase kit (Promega) according to the manufacturer's instructions. The pBVIx-Luc reporter construct and pcDNA3-NOD1-HA were kindly provided by G. Nuñez (University of Michigan Medical School, Ann Arbor, MI).

RESULTS

Generation of CARD6$^{-/-}$ mice. CARD6$^{+/fl}$ ES cells were generated by homologous recombination using a targeting vector in which exon 4 of the murine CARD6 gene was flanked by loxP sites (Fig. 1A). CARD6 exon 4 encodes 77% of the protein sequence and all of the features shared with IFNiGTPases. These ES clones were used to generate CARD6$^{+/-}$ mice as described in Materials and Methods. Successful gene targeting was confirmed by Southern blot analysis (Fig. 1B), and the loss of CARD6 mRNA expression in CARD6$^{-/-}$ mice was demonstrated by RT-PCR (Fig. 1C). Western blotting with the anti-moCARD6 antibody (7), which recognizes a peptide in the N-terminal region of the protein sequence encoded by exon 4, confirmed the loss of CARD6 protein expression (Fig. 1D). Unexpectedly, the protein specifically detected by the anti-moCARD6 antibody in WT bone marrow exhibited an apparent molecular mass of approximately 50 kDa (ΔCARD6S). This protein is significantly smaller than the (predicted) 132-kDa CARD6 protein that is detected in WT thymocytes (Fig. 1D). This finding suggests that CARD6 gene products are subject to differential processing, such that different CARD6 isoforms appear in different tissues. Among B cells, granulocytes, and erythroid cells, which were isolated from bone marrow with antibodies recognizing the CD19, Gr-1, and Ter119 markers, respectively, the ~50-kDa CARD6 variant was detected only in granulocytes (data not shown). Overall, CARD6$^{-/-}$ mice were viable and fertile, did not show any gross developmental abnormalities, and were born at the expected Mendelian ratio (Fig. 1E). Flow cytometric analyses did not detect any developmental abnormalities in thymocytes, granulocytes, macrophages, natural killer cells, or in various T- and B-cell subsets (Fig. 1F; also data not shown).

Many CARD proteins function in multiprotein complexes to regulate programmed cell death. Moreover, the CARD of CARD6 is most closely related to the CARD of apoptosis repressor with CARD (ARC), a molecule that physically interacts with various mediators of programmed cell death and

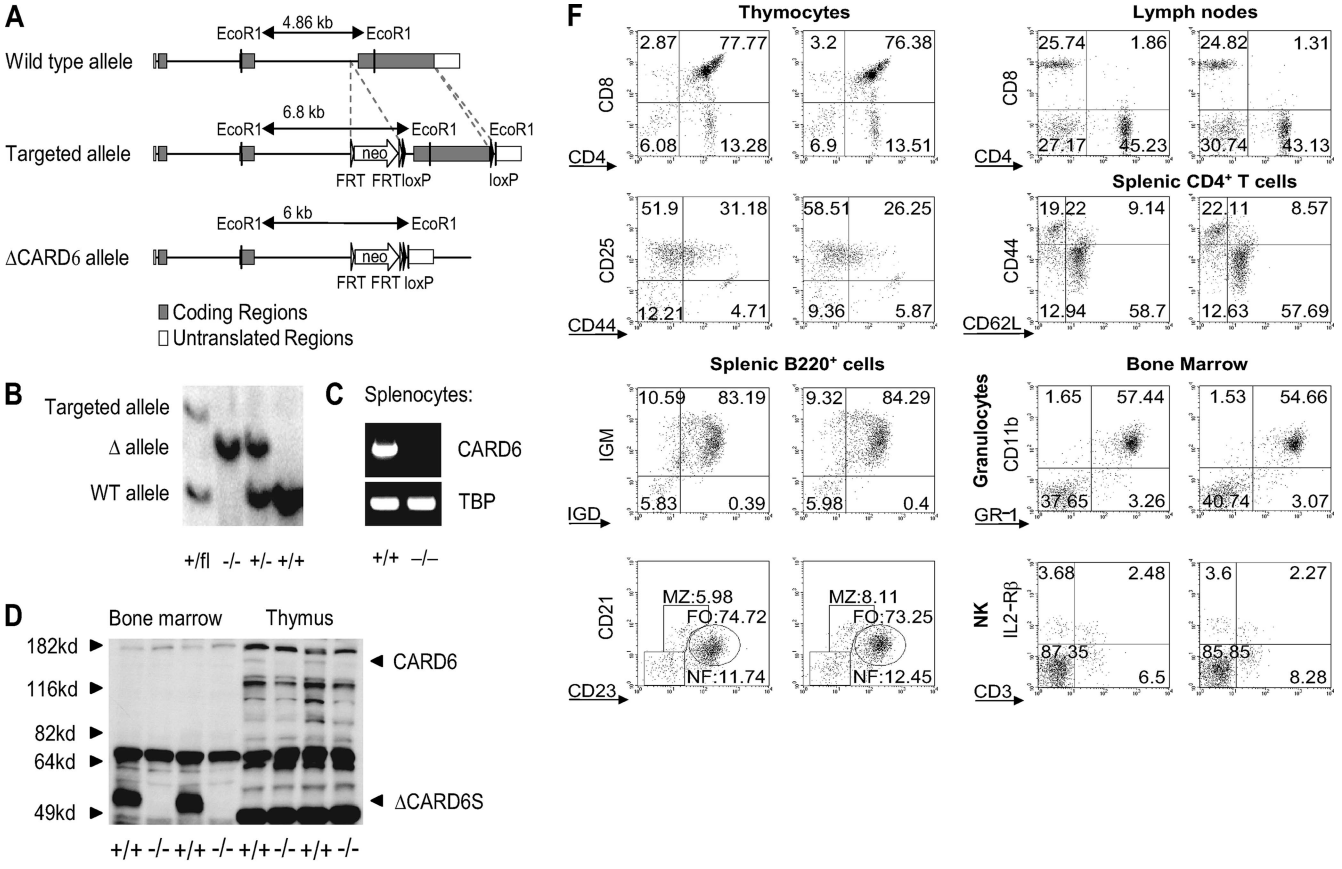

E

	+/+	+/–	–/–
Total	47	97	52
%	24	49.5	26.5

FIG. 1. Generation of CARD6-deficient mice. (A) Diagram of the CARD6 WT locus, the targeted allele, and the ΔCARD6 allele lacking the loxP-flanked gene fragment. The EcoRI restriction sites and the FLP and Cre recombination target sites (FRT/loxP) are indicated. (B) Southern blot analysis of EcoRI-digested genomic DNA identifies mice of all expected genotypes. (C) Lack of CARD6 RNA expression in CARD6$^{-/-}$ mice. Splenocyte RNA isolated from CARD6$^{+/+}$ and CARD6$^{-/-}$ mice was subjected to RT-PCR analysis using primer pairs specific for CARD6 or TBP (control). (D) Western blot analysis of CARD6$^{+/+}$ and CARD6$^{-/-}$ bone marrow and thymocytes, confirming the absence of the ΔCARD6S variant and the WT CARD6 protein, respectively. (E) Total number and relative distribution (%) of CARD6$^{+/+}$, CARD6$^{+/-}$, and CARD6$^{-/-}$ offspring derived from CARD6$^{+/-}$ intercrosses. (F) Normal numbers of thymocyte subsets, natural killer cells, granulocytes, and various T- and B-cell subsets in the absence of CARD6. Flow cytometric analyses of cells in the thymus, lymph nodes, spleen, and bone marrow of CARD6$^{+/+}$ and CARD6$^{-/-}$ mice. Numbers indicate the percentages of cells within the quadrants or regions. Dot plots show one result, representative of five mice per genotype.

interferes with extrinsic and intrinsic apoptotic pathways (6). We therefore examined a range of chemical and physical apoptosis-inducing agents to determine whether CARD6 might be involved in apoptotic regulation. We treated thymocytes with FasL, anti-CD3, staurosporine, γ-irradiation, or UV irradiation, but no differences in apoptosis were detected between WT and CARD6$^{-/-}$ thymocytes (Fig. 2). These results indicate that CARD6 is not involved in the regulation of apoptosis.

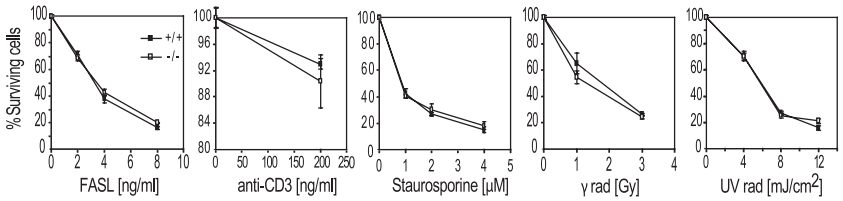

FIG. 2. Normal susceptibility to apoptosis of CARD6$^{-/-}$ thymocytes. Freshly isolated CARD6$^{+/+}$ and CARD6$^{-/-}$ thymocytes were treated with the indicated amounts of FasL, anti-CD3, or staurosporine or were exposed to the indicated doses of γ-irradiation or UV irradiation. Results shown are the mean percentages of surviving cells normalized to spontaneous cell death in untreated controls 24 h after treatment. Spontaneous cell death was similar in +/+ and −/− thymocytes. Data shown are the mean percent surviving cells ± standard deviations for triplicate samples. One trial, representative of at least three independent experiments, is presented for each stimulus.

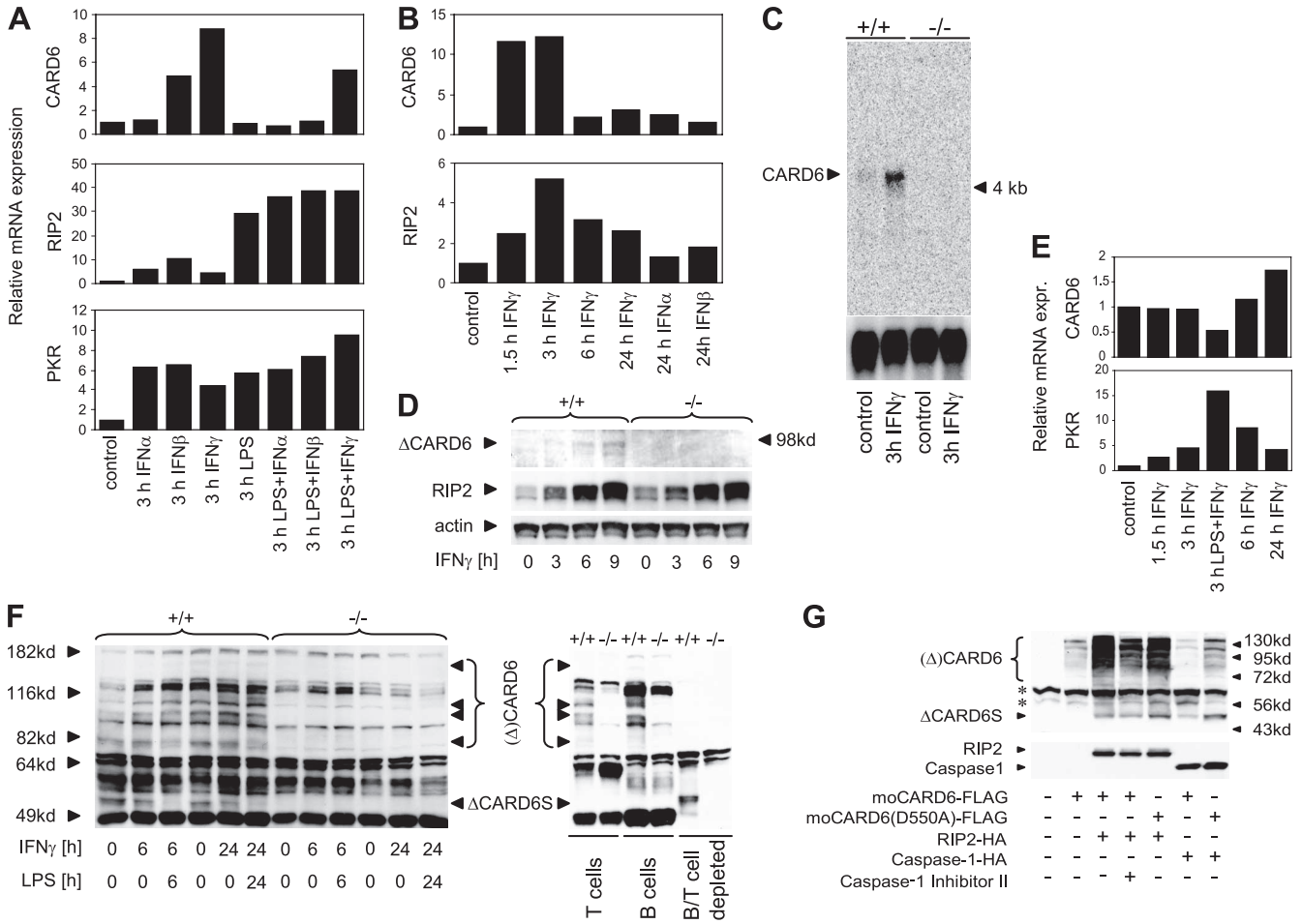

FIG. 3. Regulation of CARD6 expression in BMDMs and splenocytes by IFNs and LPS. (A) Relative CARD6, RIP2, and PKR mRNA expression in BMDMs. BMDMs were stimulated for 3 h with 100 U ml^{-1} IFN-α or IFN-β, 50 ng ml^{-1} IFN-γ, or 100 ng ml^{-1} LPS or the indicated combinations of IFNs and LPS. RNA expression was measured by quantitative real-time PCR analysis. Results shown are mRNA levels relative to mRNA levels in unstimulated controls. (B) CARD6 mRNA induction by IFN-γ is rapid and transient. BMDMs were stimulated for the indicated times with 100 U ml^{-1} IFN-γ, IFN-α, or IFN-β. Relative mRNA expression was determined as for panel A. (C) Confirmation of CARD6 mRNA induction. $CARD6^{+/+}$ and $CARD6^{-/-}$ BMDMs were left untreated or stimulated with IFN-γ for 3 h, and CARD6 RNA expression was detected by Northern blotting. (D) Upregulation of the ΔCARD6 protein variant in WT BMDMs. $CARD6^{+/+}$ and $CARD6^{-/-}$ BMDMs were stimulated with IFN-γ for the indicated times, and extracts were subjected to Western blotting to detect CARD6, RIP2, and actin. (E) Relative CARD6 and PKR mRNA expression in splenocytes. Freshly isolated $CARD6^{+/+}$ splenocytes were stimulated with IFN-γ in the absence or presence of LPS for the indicated times, and relative mRNA expression was determined as for panel A. (F) CARD6 protein expression in splenocytes. Left panel, $CARD6^{+/+}$ splenocytes were incubated with IFN-γ in the absence or presence of LPS for the indicated times, and the expression of the (Δ)CARD6 and ΔCARD6S proteins was determined by Western blotting. Right panel, base levels of CARD6 protein expression were determined in unstimulated WT splenic T cells and B cells and in WT splenocytes depleted of T and B cells. Protein extracts from $CARD6^{-/-}$ splenocytes are included as controls in both panels. (G) Proteolytic CARD6 degradation is not altered by a mutation in a putative caspase-1 cleavage site or by caspase-1 inhibition. 293T cells were transfected with empty vector or the indicated CARD6 expression constructs in the absence or presence of expression constructs for HA-tagged RIP2 or caspase-1. Where indicated, cells were also treated with caspase-1 inhibitor II (Calbiochem) at a final concentration of 10 μM. Cells were lysed at 36 h posttransfection, and expression levels of exogenous CARD6 (upper panel) or HA-tagged RIP2 and caspase-1 (lower panel) were analyzed using anti-moCARD6 antibody or anti-HA antibody, respectively. Results shown are from one trial, representative of at least three (A, B, D, and E) or two (F and G) independent experiments. ∗, cross-reactive bands.

CARD6 expression is induced by IFN-β and IFN-γ but inhibited by LPS. Because CARD6 shares structural features with members of the IFNiGTPase superfamily, we tested whether CARD6 expression was regulated by IFNs. Interestingly, CARD6 mRNA expression was increased 5- to 10-fold in WT BMDMs stimulated with IFN-β and IFN-γ for 3 h, whereas IFN-α and LPS had no effect (Fig. 3A, upper panel). Surprisingly, LPS treatment inhibited CARD6 RNA induction by IFN-β or IFN-γ, in contrast to LPS's enhancement of RIP2 and PKR expression induced by IFN-β or IFN-γ (Fig. 3A, lower panels). A time course analysis revealed that CARD6 mRNA was maximally induced after 1.5 h of IFN-γ stimulation but had returned to near-basal levels by 6 h (Fig. 3B, upper panel). The observation that CARD6 mRNA induction by IFN-γ is rapid and transient suggests that this transcriptional upregulation is an event that lies directly downstream of IFN receptor engagement. IFN-γ treatment of WT BMDMs also resulted in the upregulation of a single full-length CARD6

RNA band (Fig. 3C) and a CARD6 protein variant of approximately 95 kDa (Fig. 3D, upper panel). This 95-kDa protein was also detected in splenocytes (Fig. 3F). Consistent with the finding that CARD6 interacts with RIP2 (7), RIP2 mRNA and protein expression were markedly upregulated by IFN-γ with kinetics similar to those of CARD6 induction (Fig. 3B, lower panel, and Fig. 3D, middle panel).

In contrast to BMDMs, IFN-γ-treated WT splenocytes showed CARD6 mRNA expression that was stable for 3 h but then steadily increased after 6 h and 24 h (Fig. 3E, upper panel). An array of proteins of 50 kDa (ΔCARD6S) or >50 to 130 kDa [(Δ)CARD6] was specifically detected by the CARD6 antibody in WT splenocytes but not in CARD6$^{-/-}$ splenocytes (Fig. 3F, left panel). Fractionation of the total WT splenocyte population revealed that expression of the ΔCARD6S variant was restricted to the non-B-, non-T-cell subpopulation. Conversely, larger protein variants were expressed only in B and T cells (Fig. 3F, right panel). While CARD6 protein expression in WT splenocytes remained stable for 24 h after IFN-γ stimulation (Fig. 3F), LPS cotreatment downregulated the expression of both CARD6 mRNA (Fig. 3E, upper panel) and the ΔCARD6S protein (Fig. 3F, left panel).

The presence of a single CARD6 mRNA variant in IFN-γ-stimulated BMDMs, as well as in tissues in which the full-length CARD6 mRNA is known to be expressed (7), implies that truncated CARD6 protein variants are generated by proteolytic processing. To determine whether mouse CARD6 is a potential caspase target, we used the ExPASy PeptideCutter tool to scan the CARD6 amino acid sequence for peptide substrate sites preferred by caspase-1 to -10. This analysis revealed two potential caspase-1 cleavage sites at positions 379 and 550 of mouse CARD6. However, mutation of these sites to alanines or the use of caspase-1 (or caspase-8) inhibitors did not abolish the appearance of a ~50-kDa cleavage product of mouse CARD6 in 293T cells overexpressing CARD6 mRNA in the presence of exogenous RIP2 or caspase-1 (Fig. 3G; also data not shown). These findings corroborate previous coimmunoprecipitation experiments in which no physical interactions between CARD6 and caspase-1, -2, -8, -9, -11, or -12 were detected (unpublished results). Taken together, our results indicate that CARD6 expression is regulated by IFN-β and IFN-γ and that the CARD6 protein undergoes caspase-independent proteolytic processing.

Normal T- and B-cell responses in absence of CARD6. The presence of CARD6 protein in T and B lymphocytes and the possible involvement of RIP2 in TCR signaling (3, 17, 29) prompted us to investigate whether CARD6 was required for optimal T- or B-cell activation. A previous report indicated that RIP2 may interact directly with BCL10, an adaptor molecule that links TCR engagement to NF-κB activation (29). T-cell activation induced by anti-CD3 antibody (with or without anti-CD28 costimulation) is abolished in BCL10$^{-/-}$ T cells (30) and was initially reported to be impaired in RIP2$^{-/-}$ cells (3, 17, 29). In contrast, stimulation of T cells with TPA, a mitogen that activates protein kinase C directly and bypasses proximal antigen receptor signaling, is abrogated in BCL10$^{-/-}$ cells (30) but is not affected in RIP2$^{-/-}$ cells (17). Since CARD6 interacts with RIP2 and enhances NF-κB activation mediated by exogenous RIP2 and BCL10 (7), we wondered if CARD6 was implicated in TCR signaling. We subjected CARD6$^{-/-}$ T cells to stimulation with anti-CD3ε antibody (with or without anti-CD28) or treated them with TPA and ionomycin and found that the mutant cells proliferated normally (Fig. 4A, upper panels). We then examined CARD6's role in B-cell expansion in response to B-cell receptor (BCR) or TLR9 engagement. Consistent with previous findings that RIP2 is not involved in BCR or TLR9 signaling (3, 17), CARD6$^{-/-}$ B cells displayed no defects in in vitro B cell stimulation in response to anti-IgM, anti-IgM plus anti-CD40, or CpG. Proliferation induced by LPS treatment was also normal in CARD6$^{-/-}$ B cells (Fig. 4A, lower panels).

Western blotting confirmed that IκBα degradation and ERK1/2 phosphorylation were induced normally in CARD6$^{-/-}$ T cells in response to TPA (Fig. 4B, upper left panels) or anti-CD3ε plus anti-CD28 (Fig. 4B, lower left panels). Likewise, the activation of p38 and Jun N-terminal protein kinase (JNK) by TPA was not impaired in CARD6$^{-/-}$ T cells (Fig. 4B, upper left panels). Similarly, various signaling molecules downstream of the BCR showed normal activation in CARD6$^{-/-}$ B cells subjected to TPA stimulation (Fig. 4B, upper right panels) or anti-IgM treatment (Fig. 4B, lower right panels).

It has been reported that IFN-γ production is severely impaired in RIP2$^{-/-}$ T_H1 cells stimulated with anti-CD3, IL-12, or IL-18 (3, 17). We therefore tested whether CARD6 was required for the execution of T_H1 responses in in vitro-differentiated splenocytes. In response to anti-CD3 stimulation, T_H1- and T_H2-differentiated CARD6$^{-/-}$ splenocytes exhibited normal IFN-γ and IL-4 secretion, respectively (Fig. 4C, upper panels). In addition, T_H1-differentiated CARD6$^{-/-}$ splenocytes showed normal IFN-γ production in response to IL-18, IL-12, or a combination of both cytokines (Fig. 4C, lower panels). Taken together, these results indicate that CARD6 is not essential for T- or B-cell activation, for in vitro T_H1/T_H2 differentiation, or for cytokine production.

CARD6 is not required for NOD or TLR signaling in BMDMs. Immune responses are largely orchestrated by cytokines and chemokines secreted by macrophages. Macrophages produce these mediators upon recognition of pathogen-associated molecular patterns (PAMPs) by extracellular and intracellular receptors, such as TLRs or NODs, respectively. Analyses of RIP2$^{-/-}$ mice initially indicated that RIP2 was important for optimal TLR2, TLR3, and TLR4 signaling but not for TLR9 signaling (17). The same study also confirmed that RIP2 is absolutely required for NF-κB activation triggered by the engagement of NOD1 or NOD2 (17). However, recent studies have challenged the involvement of RIP2 in TLR signaling (12a, 28). In agreement with the latter analyses, we did not observe a defect in TNF-α, IL-6, or IL-1β secretion by CARD6$^{-/-}$ BMDMs stimulated with LPS, Pam3-CSK4, poly(IC), or CpG, which are ligands for TLR4, TLR2, TLR3/MDA-5/RIG-1, and TLR9, respectively (Fig. 5A). Thus, CARD6 is not required for TLR- or MDA-5/RIG-1-induced cytokine production. We then examined cytokine production in response to NOD2 engagement by MDP or NOD1 engagement by iE-DAP. Since stimulation of BMDMs with MDP or iE-DAP alone is not sufficient to elicit a measurable cytokine response, we treated BMDMs with MDP or iE-DAP plus very small amounts of LPS and assessed cytokine production in the presence of the two stimuli compared to production following stimulation with LPS alone. Again, there was no difference in

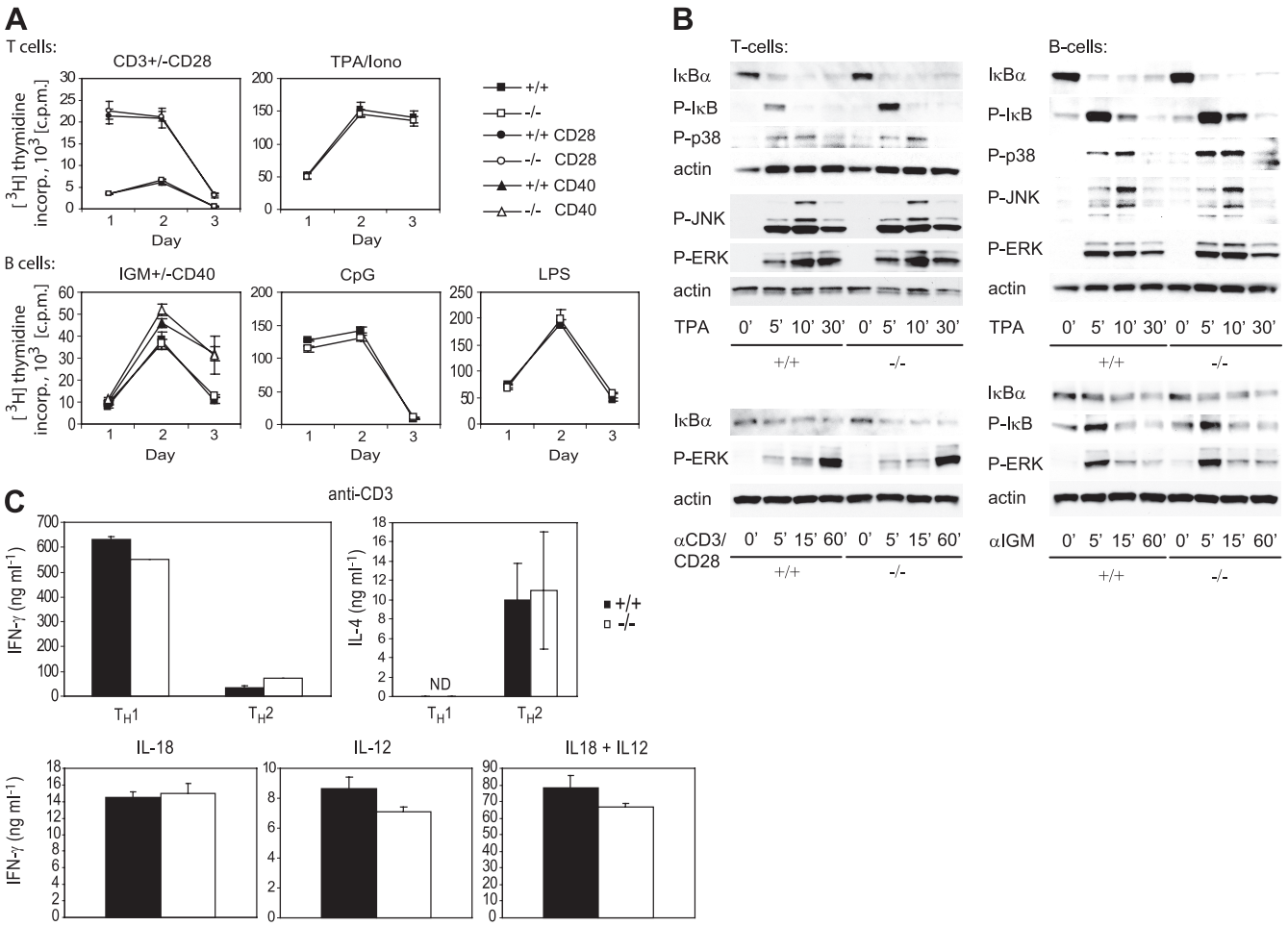

FIG. 4. Normal T- and B-cell responses in CARD6$^{-/-}$ mice. (A) Normal proliferation. Upper panels, purified CARD6$^{+/+}$ and CARD6$^{-/-}$ splenic CD4^{+} T cells were stimulated for the indicated times with plate-bound anti-CD3 in the presence or absence of anti-CD28 or with TPA-ionomycin. Lower panels, purified splenic B cells were stimulated for the indicated times with soluble anti-IgM, anti-IgM plus anti-CD40, CpG, or LPS. For both sets of panels, proliferation was measured by [^{3}H]thymidine incorporation. Results are presented as the mean [^{3}H]thymidine incorporation ± the standard deviation for triplicate samples after an 8-h pulse and are from one trial representative of at least three independent experiments. (B) Normal IκBα degradation and MAPK activation. Left panels, CARD6$^{+/+}$ and CARD6$^{-/-}$ lymph node T cells were stimulated for the indicated times with 50 ng ml^{-1} TPA or anti-CD3 plus anti-CD28 (10 μg ml^{-1} each) cross-linked with anti-hamster IgG (20 μg ml^{-1}). Right panels, splenic B cells were stimulated for the indicated times with 50 ng ml^{-1} TPA or anti-IgM (10 μg ml^{-1}). For both sets of panels, IκBα degradation, phosphorylation of IκBα, p38, ERK1/2, and JNK, and actin protein levels were determined by Western blotting. (C) Normal T_H1 and T_H2 responses. CARD6$^{+/+}$ and CARD6$^{-/-}$ splenocytes were cultured under T_H1 differentiation conditions and restimulated with anti-CD3 (upper left panel), IL-18, IL-12, or a combination of IL-12 and IL-18 (lower panels). IFN-γ production was determined by ELISA. Results shown are the mean IFN-γ production ± standard deviation and are single trials representative of at least three independent experiments. Upper right panel, CARD6$^{+/+}$ and CARD6$^{-/-}$ splenocytes were cultured under T_H2 differentiation conditions and restimulated with anti-CD3. IL-4 production was determined by ELISA. Results shown are the mean IL-4 production ± standard deviation for three independent experiments.

the cytokine responses exhibited by stimulated WT and CARD6$^{-/-}$ BMDMs (Fig. 5B). Moreover, short-term degradation of IκBα and ERK1/2 activation in response to LPS or MDP alone were comparable in WT and CARD6$^{-/-}$ BMDMs (Fig. 5C). Finally, JNK and p38 activation induced by LPS was comparable in WT and CARD6$^{-/-}$ BMDMs (Fig. 5C).

When BMDMs are treated with IFN-γ plus TLR or NOD ligands, a level of cytokine production occurs that is enhanced over that observed using the ligands alone. To determine if CARD6 was required for this IFN-γ-induced increase, we treated WT and CARD6$^{-/-}$ BMDMs with IFN-γ plus LPS, iE-DAP, MDP, or CpG or several combinations of these stimuli and assessed IL-6 production. Indeed, IFN-γ enhanced IL-6 production induced by all ligand combinations and caused a measurable cytokine response in the presence of iE-DAP and MDP, presumably via upregulation of endogenous RIP2; however, this enhancement did not depend on CARD6 (Fig. 5D). To further confirm that CARD6 is not required for NOD1 signaling, we overexpressed NOD1 in WT and CARD6$^{-/-}$ MEFs and monitored NF-κB activation in a luciferase reporter assay. As expected, NOD1-dependent NF-κB activation was comparable in cells of both genotypes (Fig. 5E).

TLR and NOD signaling pathways also trigger dendritic-cell maturation. To test whether CARD6 was required for this process, we treated WT and CARD6$^{-/-}$ BMDCs in vitro with MDP, LPS, or CpG to induce maturation and examined cell

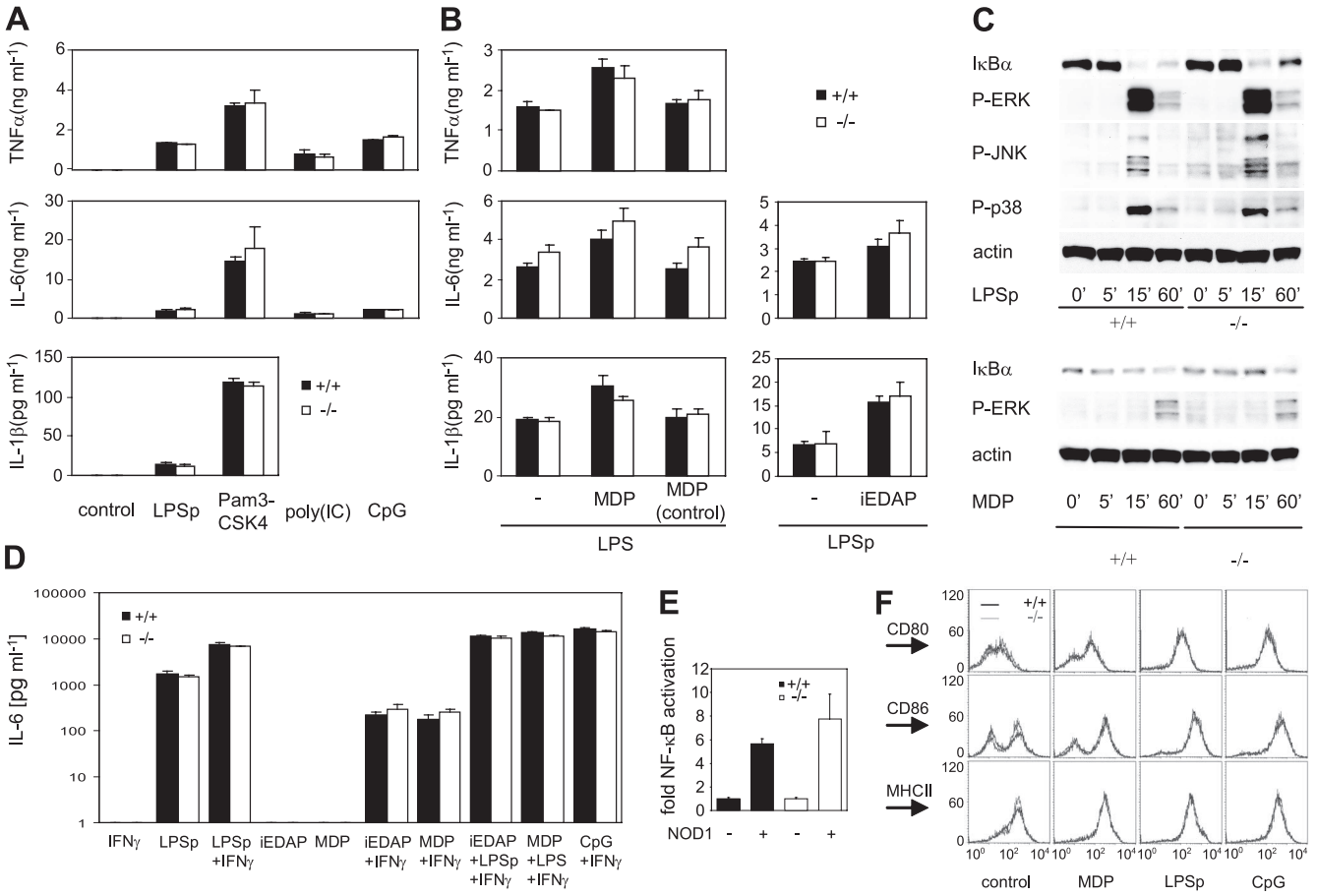

FIG. 5. Normal TLR and NOD signaling in CARD6$^{-/-}$ cells. (A and B) Normal TNF-α, IL-6, and IL-1β production. CARD6$^{+/+}$ and CARD6$^{-/-}$ BMDMs were stimulated with LPS, Pam3-CSK4, poly(IC), or CpG (A) or MDP, the MDP D-D-isomer control, or iE-DAP (B) in the presence of a low concentration of LPS. Production of TNF-α, IL-6, and IL-1β was determined by ELISA. (C) Normal IκBα degradation and MAPK activation. CARD6$^{+/+}$ and CARD6$^{-/-}$ BMDMs were stimulated with LPS (upper panels) or MDP (lower panels) for the indicated times. IκBα degradation, phosphorylation of ERK1/2, p38, and JNK, and actin protein levels were determined by Western blotting. (D) Normal IL-6 production in the presence of IFN-γ. CARD6$^{+/+}$ and CARD6$^{-/-}$ BMDMs were stimulated with IFN-γ, LPSp (low concentration), iE-DAP, or MDP or the indicated combinations of these stimuli or CpG plus IFN-γ, and IL-6 production was determined by ELISA. (E) Normal NF-κB activation. CARD6$^{+/+}$ and CARD6$^{-/-}$ MEFs were cotransfected with empty vector or the pcDNA3-NOD1-HA expression construct plus the pBVIx-Luc and pRL-TK reporters, and the increase in NF-κB activation was determined. (F) Normal DC maturation in response to NOD2 and TLR stimulation. BMDCs from CARD6$^{+/+}$ and CARD6$^{-/-}$ mice were stimulated for 24 h with MDP, LPSp, or CpG as described in Materials and Methods. CD11c-positive cells were analyzed for cell surface levels of CD80, CD86, and MHCII by flow cytometry. Results, shown as bar graphs, are the means of normalized values ± standard deviations for triplicate cultures and are representative of at least three (A, B, and D) or two (E) independent experiments. Results shown in panels C and F are one trial representative of at least two or three independent experiments, respectively.

surface levels of two key costimulatory molecules, CD80 and CD86, as well as levels of major histocompatibility class II (MHCII) molecules. WT and CARD6$^{-/-}$ BMDCs exhibited identical levels of all markers (Fig. 5F). Taken together, our results strongly indicate that CARD6 is not required for TLR or NOD signaling.

CARD6 deficiency does not result in loss of host resistance to infection with *Salmonella*, *Listeria*, *Candida albicans*, LCMV, or MAV-1. We next focused on the structural relatedness of CARD6 to the IFNiGTPase superfamily in an attempt to determine the physiological function of CARD6. Many members of the IFNiGTPase superfamily are involved in host defense-related sequestration and trafficking mechanisms, functions that would be consistent with CARD6's associations with the microtubule network and aggresomes (7). A prominent example of an IFNiGTPase is the p47 GTPase Irgm1 (or LRG-47), which mediates antimicrobial phagosome remodelling upon infection of cells with pathogens that have a vacuolar lifestyle (4, 23, 31). More recently Irgm1 has been implicated in IFN-γ-mediated induction of autophagy (12). Autophagy not only is an important cell-autonomous host defense mechanism but also is involved in acquired immunity, because it promotes MHCII presentation of pathogen-derived peptides (5). To test whether CARD6 was required for pathogen-specific cell-autonomous or systemic immune responses, we exposed WT and CARD6$^{-/-}$ mice to various pathogens and monitored the animals for survival, pathogen loads in organs, and blood cytokine levels. To determine susceptibility to bacterial infection, we injected WT and CARD6$^{-/-}$ mice with the gram-negative bacterium *Salmonella enterica* serovar Typhimurium (Fig. 6A)

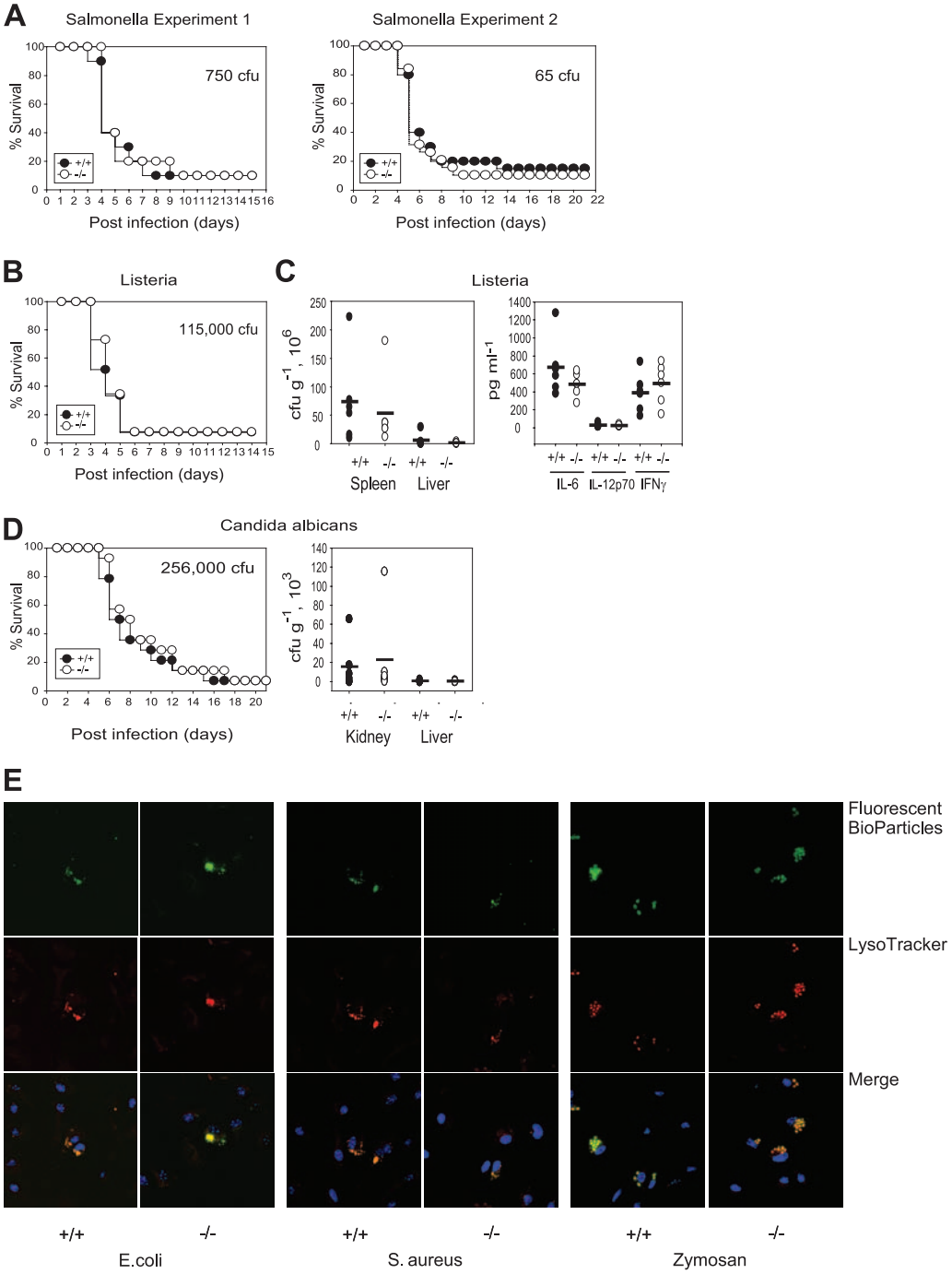

FIG. 6. CARD6$^{-/-}$ mice show normal susceptibility to infection. (A) Survival curves of CARD6$^{+/+}$ and CARD6$^{-/-}$ mice after intraperitoneal injection of the indicated numbers (CFU) of *Salmonella enterica* serovar Typhimurium bacteria (n = 10 mice/group [left panel] or n = 20 WT and 19 KO mice [right panel]). (B) Survival curve of CARD6$^{+/+}$ and CARD6$^{-/-}$ mice after intravenous injection of the indicated number of *Listeria monocytogenes* bacteria (n = 27 WT and 26 knockout mice). (C) Equivalent bacterial loads and blood cytokine levels. CARD6$^{+/+}$ and CARD6$^{-/-}$ mice (n = 6/group) were injected intravenously with 108,000 CFU *Listeria monocytogenes*, and spleen, liver, and blood samples were taken at 3 days postinfection. Bacterial loads in organs (left) and serum IL-6, IL-12p70, and IFN-γ levels (right) were determined as described in Materials and Methods. (D) Equivalent survival and organ loads after fungal infection. Left panel, survival curves of CARD6$^{+/+}$ and CARD6$^{-/-}$ mice (n = 14/group) after intravenous injection of the indicated amount of *Candida albicans* yeast. Right panel, CARD6$^{+/+}$ and CARD6$^{-/-}$ mice were intravenously injected with 79,000 CFU *Candida albicans*, and organ loads in kidney and liver were determined at 3 days postinfection. (E) Normal phagolysosomal fusion. BMDMs from CARD6$^{+/+}$ and CARD6$^{-/-}$ mice were stimulated with IFN-γ, labeled with Lyso-Tracker Red, and exposed to *Escherichia coli*, *Staphylococcus aureus*, or zymosan A BioParticles conjugated to Alexa Fluor 488. After 1 h of incubation, the cells were fixed and bound fluorochromes were visualized.

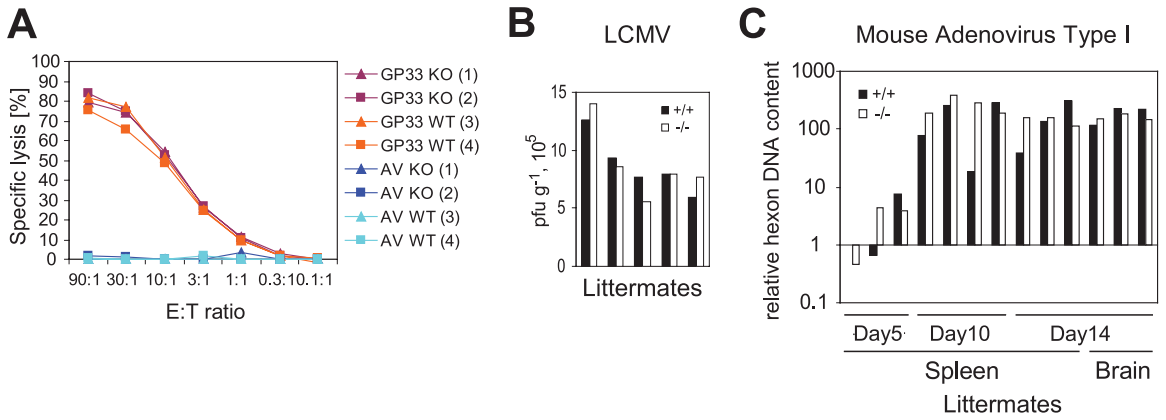

FIG. 7. (A) Normal CTL generation in response to LCMV. Two pairs of CARD6$^{+/+}$ and CARD6$^{-/-}$ littermates were infected with 2,000 PFU LCMV, and splenocytes were isolated at 8 days postinfection and evaluated for cytotoxicity against GP33-pulsed EL4 cells. (B) Comparable LCMV titers. CARD6$^{+/+}$ and CARD6$^{-/-}$ littermates were intravenously infected with 2,000 PFU LCMV, and LCMV titers in spleens were determined at 3 days postinfection. (C) Equivalent response to MAV-1. CARD6$^{+/+}$ and CARD6$^{-/-}$ littermates were infected intraperitoneally with 1,000 PFU MAV-1, and relative MAV-1 DNA expression in spleens and brains was determined by quantitative PCR at the indicated days postinfection.

or the gram-positive bacterium *Listeria monocytogenes* (Fig. 6B). No significant differences in survival rates were observed. Bacterial loads in spleen and liver and levels of IL-6, IL-12p70, and IFN-γ in serum of Listeria-infected WT and CARD6$^{-/-}$ mice were also comparable at 3 days postinfection (Fig. 6C). The IL-1 serum concentrations were below detection levels in mice of both genotypes in this experiment. Similar results were obtained when we infected WT and CARD6$^{-/-}$ mice with *Candida albicans* and monitored survival and fungal loads in kidney and liver tissue at day 3 postinfection (Fig. 6D). Thus, CARD6$^{-/-}$ mice do not show enhanced susceptibility to either bacterial or fungal infections.

To quantify the uptake of bacteria and zymosan by macrophages in vitro, we incubated WT and CARD6$^{-/-}$ BMDMs with fluorescently labeled, heat-inactivated *Escherichia coli*, *Staphylococcus aureus*, or zymosan as described in Materials and Methods. Using fluorescence-activated cell sorting, we determined that CARD6$^{-/-}$ macrophages carried out normal phagocytosis of these entities whether or not they were preincubated with opsonizing antibodies (data not shown). LysoTracker staining of WT and CARD6$^{-/-}$ BMDMs exposed to the fluorescently labeled pathogen particles confirmed that phagolysosomal fusion proceeded normally in the absence of CARD6 (Fig. 6E).

To assess the susceptibility of CARD6$^{-/-}$ mice to viral infections, we infected WT and CARD6$^{-/-}$ mice intravenously with a low dose of LCMV. CARD6$^{-/-}$ mice generated a normal number of functional LCMV-specific cytotoxic T lymphocytes (CTLs) (Fig. 7A; also data not shown), and comparable viral titers were present in WT and CARD6$^{-/-}$ spleens at 3 days postinfection (Fig. 7B). These data indicate that the innate immune response against RNA viruses such as LCMV is not impaired in the absence of CARD6.

The host cytoskeleton provides DNA viruses with a means of reaching the nucleus, where replication can take place (10). Because CARD6 is associated with the host cytoskeleton, we tested the susceptibility of CARD6$^{-/-}$ mice to infection by the DNA virus MAV-1. Infection of WT C57BL/6 mice with MAV-1 is known to cause dose-dependent encephalomyelitis (11). We injected sex-matched WT and CARD6$^{-/-}$ littermates intraperitoneally with 1,000 PFU MAV-1 and used real-time PCR to quantify the viral DNA content of spleens and brains at 5 to 14 days postinfection (Fig. 7C). As observed for the other classes of pathogens examined, MAV-1 infection progressed at essentially the same rate in mice of both genotypes. Taken together, these data demonstrate that CARD6$^{-/-}$ mice do not differ from their WT counterparts in their susceptibility to a wide range of pathogens.

DISCUSSION

Our previously reported cloning and biochemical characterization of CARD6 led to a working hypothesis that CARD6 might be a microtubular sequestration or transport molecule that is an effector or regulator of RIP2. In agreement with CARD6's relatedness to the IFNiGTPases, we demonstrate here that CARD6 mRNA is indeed upregulated by IFN-β and IFN-γ in a transient fashion. Importantly, this upregulation of CARD6 mRNA correlates with the upregulation of RIP2 expression induced by IFNs, a result demonstrated for the first time in this study.

RIP2 is an essential mediator of NOD-induced NF-κB activation (3, 14, 17). Gene ablation studies have indicated that RIP2 is also important for optimal signaling by the TCR and several TLRs and for T_H1 responses to IL-12 and IL-18 (3, 17, 29). However, these findings have recently been challenged and attributed to undetected activation of NOD1 or NOD2 (9, 12a, 21, 28, 37). Thus, our finding that CARD6 is not involved in any of the TLR- or TCR-triggered pathways is consistent with the observation that CARD6 is not involved in any known aspect of NOD signaling. Moreover, treatment of WT BMDMs or splenocytes with LPS, a cell wall component of gram-negative bacteria, induced suppression (rather than upregulation) of CARD6 mRNA and protein in our study. If CARD6 were truly important for defense against bacteria, one would expect an additive effect of IFNs and LPS on CARD6 mRNA levels, such as occurs for RIP2 mRNA levels in cells exposed to LPS and IFN-γ. It is possible,

however, that IFNs and LPS (and eventually other PAMPs) may act in concert to determine the timing of CARD6 expression, which may in turn be critical for CARD6's function.

Our analysis of tissue expression of CARD6 implies that truncated protein variants exist in WT spleen, BMDMs, and bone marrow. This processing of CARD6 may provide an additional level of regulation that determines the functional consequences of CARD6 transcriptional upregulation. The finding that the related ARC protein binds to caspase-8 and caspase-2 (15, 18, 20) would support an interaction between CARD6 and caspases. However, despite the identification of potential caspase cleavage sites in CARD6, CARD6 does not appear to physically interact with caspases. It remains possible that the acidic region of CARD6 participates in caspase regulation in a manner that is controlled by posttranslational modifications.

The IFNiGTPases play important roles in cell-autonomous immune responses against various pathogens (24). However, despite the structural relatedness of CARD6 to the IFNiGTPases, CARD6$^{-/-}$ mice were no more susceptible than WT mice to bacterial, fungal, or viral infections and showed no defects in antigen processing or presentation during LCMV infection. The uptake of fluorescently labeled pathogen particles and phagolysosomal fusion also proceeded normally in the absence of CARD6. It is possible, however, that CARD6 plays a role in immune defense against pathogens with characteristics different from those tested in our study. These characteristics could include the presence of distinct pathogen-specific PAMPs or the absence of immune evasion mechanisms that target CARD6 function. Alternatively, the genetic background of our infected mice (C57BL/6) may have influenced their susceptibility to infection. C57BL/6 mice are highly susceptible to *Mycobacterium*, *Leishmania*, and *Salmonella* infections due to a mutation of the Nramp1 gene, which encodes an antimicrobial metal transporter that functions at the membrane of macrophage phagosomes (8, 26). Thus, *Salmonella* could have an infectious advantage in our CARD6$^{-/-}$ mice that might not be manifested in CARD6$^{-/-}$ mice of a different genetic background. The finding that the CARD6 protein sequence is not highly conserved between humans and mice (7) suggests that the functionality of the CARD6 pathway itself may be influenced by genetic variability within a species. Thus, CARD6 may play a very subtle role in the fine-tuning of immune responses, a role that ultimately does not determine their overall effectiveness. It is well known that the magnitude of the innate immune response needs to be tightly regulated to avoid septic shock while preventing sepsis (33).

Although we could not demonstrate a function for CARD6 in responses against the pathogens tested in this study, the observed regulation of CARD6 by interferons, as well as CARD6's structure and its interaction with RIP2, strongly imply that CARD6 plays a role in immune defense. Thus, further characterization of CARD6 function and its underlying mechanisms may contribute to the development of novel strategies for the treatment of infectious disease. The rise of multidrug-resistant pathogens has made it very clear that such new approaches are desperately needed.

ACKNOWLEDGMENTS

We thank Z. Hao for Cre deleter mice; A. Itie for blastocyst injections; T. H. Watts (University of Toronto), J. B. Anderson (University of Toronto), J. H. Brumell (Hospital for Sick Children, Toronto), R. J. Ulevitch (The Scripps Research Institute, La Jolla, CA), G. Nuñez (University of Michigan, Ann Arbor), and K. R. Spindler (University of Michigan, Ann Arbor) for reagents; and M. Saunders for scientific editing.

This work was supported by the Terry Fox Program of the National Cancer Institute of Canada (T.W.M.) and in part by a fellowship from the Cancer Research Institute, New York, NY (A.D.).

REFERENCES

1. **Battegay, M., S. Cooper, A. Althage, J. Banziger, H. Hengartner, and R. M. Zinkernagel.** 1991. Quantification of lymphocytic choriomeningitis virus with an immunological focus assay in 24- or 96-well plates. J. Virol. Methods **33:**191–198.
2. **Bouchier-Hayes, L., and S. J. Martin.** 2002. CARD games in apoptosis and immunity. EMBO Rep. **3:**616–621.
3. **Chin, A. I., P. W. Dempsey, K. Bruhn, J. F. Miller, Y. Xu, and G. Cheng.** 2002. Involvement of receptor-interacting protein 2 in innate and adaptive immune responses. Nature **416:**190–194.
4. **Collazo, C. M., G. S. Yap, G. D. Sempowski, K. C. Lusby, L. Tessarollo, G. F. Woude, A. Sher, and G. A. Taylor.** 2001. Inactivation of LRG-47 and IRG-47 reveals a family of interferon gamma-inducible genes with essential, pathogen-specific roles in resistance to infection. J. Exp. Med. **194:**181–188.
5. **Deretic, V.** 2005. Autophagy in innate and adaptive immunity. Trends Immunol. **26:**523–528.
6. **Dufner, A., and T. W. Mak.** 2006. CARD tricks: controlling the interactions of CARD6 with RICK and microtubules. Cell Cycle **5:**797–800.
7. **Dufner, A., S. Pownall, and T. W. Mak.** 2006. Caspase recruitment domain protein 6 is a microtubule-interacting protein that positively modulates NF-κB activation. Proc. Natl. Acad. Sci. USA **103:**988–993.
8. **Fortier, A., G. Min-Oo, J. Forbes, S. Lam-Yuk-Tseung, and P. Gros.** 2005. Single gene effects in mouse models of host: pathogen interactions. J. Leukoc. Biol. **77:**868–877.
9. **Fritz, J. H., L. Le Bourhis, G. Sellge, J. G. Magalhaes, H. Fsihi, T. A. Kufer, C. Collins, J. Viala, R. L. Ferrero, S. E. Girardin, and D. J. Philpott.** 2007. Nod1-mediated innate immune recognition of peptidoglycan contributes to the onset of adaptive immunity. Immunity **26:**445–459.
10. **Greber, U. F., and M. Way.** 2006. A superhighway to virus infection. Cell **124:**741–754.
11. **Guida, J. D., G. Fejer, L. A. Pirofski, C. F. Brosnan, and M. S. Horwitz.** 1995. Mouse adenovirus type 1 causes a fatal hemorrhagic encephalomyelitis in adult C57BL/6 but not BALB/c mice. J. Virol. **69:**7674–7681.
12. **Gutierrez, M. G., S. S. Master, S. B. Singh, G. A. Taylor, M. I. Colombo, and V. Deretic.** 2004. Autophagy is a defense mechanism inhibiting BCG and Mycobacterium tuberculosis survival in infected macrophages. Cell **119:**753–766.

12a. **Hall, H. T., M. T. Wilhelm, S. D. Saibil, T. W. Mak, R. A. Flavell, and P. S. Ohashi.** 12 December 2007. RIP2 contributes to Nod signaling but is not essential for T cell proliferation, T helper differentiation or TLR responses. Eur. J. Immunol. [Epub ahead of print]. doi:10.1002/eji.200737393.

13. **Haller, O., and G. Kochs.** 2002. Interferon-induced mx proteins: dynamin-like GTPases with antiviral activity. Traffic **3:**710–717.
14. **Inohara, N., T. Koseki, L. del Peso, Y. Hu, C. Yee, S. Chen, R. Carrio, J. Merino, D. Liu, J. Ni, and G. Nunez.** 1999. Nod1, an Apaf-1-like activator of caspase-9 and nuclear factor-kappaB. J. Biol. Chem. **274:**14560–14567.
15. **Jo, D.-G., J.-I. Jun, J.-W. Chang, Y.-M. Hong, S. Song, D.-H. Cho, S. M. Shim, H.-J. Lee, C. Cho, D. H. Kim, and Y.-K. Jung.** 2004. Calcium binding of ARC mediates regulation of caspase 8 and cell death. Mol. Cell. Biol. **24:**9763–9770.
16. **Klamp, T., U. Boehm, D. Schenk, K. Pfeffer, and J. C. Howard.** 2003. A giant GTPase, very large inducible GTPase-1, is inducible by IFNs. J. Immunol. **171:**1255–1265.
17. **Kobayashi, K., N. Inohara, L. D. Hernandez, J. E. Galan, G. Nunez, C. A. Janeway, R. Medzhitov, and R. A. Flavell.** 2002. RICK/Rip2/CARDIAK mediates signalling for receptors of the innate and adaptive immune systems. Nature **416:**194–199.
18. **Koseki, T., N. Inohara, S. Chen, and G. Nunez.** 1998. ARC, an inhibitor of apoptosis expressed in skeletal muscle and heart that interacts selectively with caspases. Proc. Natl. Acad. Sci. USA **95:**5156–5160.
19. **Lenaerts, L., E. Verbeken, E. De Clercq, and L. Naesens.** 2005. Mouse adenovirus type 1 infection in SCID mice: an experimental model for antiviral therapy of systemic adenovirus infections. Antimicrob. Agents Chemother. **49:**4689–4699.
20. **Li, P. F., J. Li, E. C. Muller, A. Otto, R. Dietz, and R. von Harsdorf.** 2002. Phosphorylation by protein kinase CK2: a signaling switch for the caspase-inhibiting protein ARC. Mol. Cell **10:**247–258.
21. **Lu, C., A. Wang, M. Dorsch, J. Tian, K. Nagashima, A. J. Coyle, B. Jaffee,**

T. D. Ocain, and Y. Xu. 2005. Participation of Rip2 in lipopolysaccharide signaling is independent of its kinase activity. J. Biol. Chem. **280:**16278–16283.
22. **MacMicking, J. D.** 2005. Immune control of phagosomal bacteria by p47 GTPases. Curr. Opin. Microbiol. **8:**74–82.
23. **MacMicking, J. D., G. A. Taylor, and J. D. McKinney.** 2003. Immune control of tuberculosis by IFN-gamma-inducible LRG-47. Science **302:**654–659.
24. **Martens, S., and J. Howard.** 2006. The interferon-inducible GTPases. Annu. Rev. Cell Dev. Biol. **22:**559–589.
25. **Meylan, E., and J. Tschopp.** 2005. The RIP kinases: crucial integrators of cellular stress. Trends Biochem. Sci. **30:**151–159.
26. **Mittrucker, H. W., A. Kohler, T. W. Mak, and S. H. Kaufmann.** 1999. Critical role of CD28 in protective immunity against Salmonella typhimurium. J. Immunol. **163:**6769–6776.
27. **Osoegawa, K., M. Tateno, P. Y. Woon, E. Frengen, A. G. Mammoser, J. J. Catanese, Y. Hayashizaki, and P. J. de Jong.** 2000. Bacterial artificial chromosome libraries for mouse sequencing and functional analysis. Genome Res. **10:**116–128.
28. **Park, J. H., Y. G. Kim, C. McDonald, T. D. Kanneganti, M. Hasegawa, M. Body-Malapel, N. Inohara, and G. Nunez.** 2007. RICK/RIP2 mediates innate immune responses induced through Nod1 and Nod2 but not TLRs. J. Immunol. **178:**2380–2386.
29. **Ruefli-Brasse, A. A., W. P. Lee, S. Hurst, and V. M. Dixit.** 2004. Rip2 participates in Bcl10 signaling and T-cell receptor-mediated NF-kappaB activation. J. Biol. Chem. **279:**1570–1574.
30. **Ruland, J., G. S. Duncan, A. Elia, I. del Barco Barrantes, L. Nguyen, S. Plyte, D. G. Millar, D. Bouchard, A. Wakeham, P. S. Ohashi, and T. W. Mak.** 2001. Bcl10 is a positive regulator of antigen receptor-induced activation of NF-kappaB and neural tube closure. Cell **104:**33–42.
31. **Santiago, H. C., C. G. Feng, A. Bafica, E. Roffe, R. M. Arantes, A. Cheever, G. Taylor, L. Q. Vieira, J. Aliberti, R. T. Gazzinelli, and A. Sher.** 2005. Mice deficient in LRG-47 display enhanced susceptibility to Trypanosoma cruzi infection associated with defective hemopoiesis and intracellular control of parasite growth. J. Immunol. **175:**8165–8172.
32. **Schwenk, F., U. Baron, and K. Rajewsky.** 1995. A cre-transgenic mouse strain for the ubiquitous deletion of loxP-flanked gene segments including deletion in germ cells. Nucleic Acids Res. **23:**5080–5081.
33. **Scott, A. M., and M. Saleh.** 2007. The inflammatory caspases: guardians against infections and sepsis. Cell Death Differ. **14:**23–31.
34. **Sparwasser, T., E. S. Koch, R. M. Vabulas, K. Heeg, G. B. Lipford, J. W. Ellwart, and H. Wagner.** 1998. Bacterial DNA and immunostimulatory CpG oligonucleotides trigger maturation and activation of murine dendritic cells. Eur. J. Immunol. **28:**2045–2054.
35. **Stehlik, C., H. Hayashi, F. Pio, A. Godzik, and J. C. Reed.** 2003. CARD6 is a modulator of NF-kappa B activation by Nod1- and Cardiak-mediated pathways. J. Biol. Chem. **278:**31941–31949.
36. **Tufan, N. L., Z. Lian, J. Liu, J. Pan, P. Arbuthnot, M. Kew, M. M. Clayton, M. Zhu, and M. A. Feitelson.** 2002. Hepatitis Bx antigen stimulates expression of a novel cellular gene, URG4, that promotes hepatocellular growth and survival. Neoplasia **4:**355–368.
37. **Werts, C., S. E. Girardin, and D. J. Philpott.** 2006. TIR, CARD and PYRIN: three domains for an antimicrobial triad. Cell Death Differ. **13:**798–815.